Optimization of Navigation Satellite Constellation and Lunar Monitoring Station Arrangement for Lunar Global Navigation Satellite System (LGNSS)

By Keidai IIYAMA,[1)]

[1)]*Department of Aeronautics and Astronautics, The University of Tokyo, Tokyo, Japan*

(Received February 1st, 2019)

The Lunar Global Navigation Satellite System (LGNSS) could significantly improve lunar missions' operational capability and flexibility by providing real-time, continuous, and highly accurate positioning services to lunar users. To achieve accurate user positioning, the orbit and clock bias of the navigation satellites have to be estimated accurately. An effective way to accurately estimate the orbit of navigation satellites in the lunar fixed frame is to process the psudorange data generated from the received navigation signals at lunar monitoring stations (LMSs) on the lunar surface. This paper presents a method to simulate the orbit determination error of the navigation satellites and the positioning error of the lunar user, assuming the usage of LMSs. We also propose a method to optimize the satellite constellation and LMS configuration to minimize the user positioning error. When optimizing, we reduced the number of design parameters by assuming the geometric symmetry of the navigation satellite constellation and LMS arrangement. Considering the sensitivity of the LMS arrangement and satellite constellation on the user positioning error, step by step optimization method is proposed. In the proposed method, the candidate constellation is first narrowed down by satellite visibility and PDOP analysis, followed by the LMS arrangement optimization for the selected constellations. Finally, the user positioning accuracy performance of the optimized configuration for 20 navigation satellites and 8 LMSs is analyzed. The results showed that the obtained constellation could achieve positioning errors below 10m in 3σ for the global average.

Key Words: Lunar Global Navigation Satellite System, Orbit Determination, Ground Station Arrangement, Halo Orbit, Distant Retrograde Orbit

Nomenclature

A	:	system matrix
A_z	:	z Amplitude of halo orbit
c	:	speed of light
G	:	geometry matrix
$\tilde{H}$	:	observation matrix
K	:	total number of time steps
M	:	total number of LMS
N	:	total number of satellites
n	:	number of satellites in the orbit
P	:	covariance matrix
Q	:	process noise covariance matrix
R	:	observation covariance matrix
r_p	:	perilune radius
T_p	:	revolution of orbit
U	:	total number of users
$\boldsymbol{X}$	:	state vector
$\boldsymbol{x}$	:	linearized state vector
$\boldsymbol{Y}$	:	observation vector
$\boldsymbol{y}$	:	linearized observation vector
Δt	:	clock bias
ΔX_u	:	3-d user positioning error
ϵ	:	observation noise
θ	:	latitude on lunar Surface $\in[-\pi/2,\pi/2]$, rad
μ	:	mass parameter
ρ	:	true pseudorange
$\bar{\rho}$	:	estimated pesudorange
Φ	:	state transition matrix
ϕ	:	longitude on lunar Surface $\in[-\pi,\pi]$, rad

Subscripts

d	:	DRO
h	:	halo orbit
k	:	time step
l	:	lunar monitoring station (LMS)
s	:	navigation satellite
u	:	user

1. Introduction

Recently, the interest in Moon has increased significantly as a relay point of deep space exploration and as a target for resource exploration. For advanced mission on the Moon in the future, such as an autonomous operation of robots and rovers, and for the expansion of activity area on the lunar surface, there is a need to develop a Lunar Global Navigation Satellite System (LGNSS) to provide high accuracy and real-time positional information to operators.

Carettero and Fantino (2012) studied LGNSS from a systems engineering approach.[8)] In their study, LGNSS consists of three segments as the terrestrial GNSS: space, ground, and user. The LGNSS segments have different features compared with the terrestrial GNSS, especially for the space segment and the ground segment.

The space segment refers to navigation satellite constellation. Two types of constellations are studied by previous research: Walker constellation and lunar periodic orbit (LPO) constellation. The Walker constellation consists of low lunar orbits (LLO). Wijnen and Aguera-Lopez (2018) studied the concept of LLO Walker-Delta constellation for LGNSS with cubesats.[3)] However, by using walker constellations, the required num-

ber of navigation satellites tends to be large (over 25) for full global coverage. Also, the station-keeping cost is expensive (over 50m/s per year) due to the strong perturbation in LLO. Another candidate constellation for LGNSS is constellation using LPOs that emerge in the three-body problem, such as halo orbits. Chen and Liu (2017) presented a concept of constructing a lunar far side navigation system by deploying 4 cubesats in an L2 halo orbit.[6] Circi and Romagnoli (2014) presented the LGNSS system using 4 modified halo orbits (MHOs), north and south halo orbits around L1 and L2 Lagrange points. They stated the advantages of the halo orbit-based constellation compared to the Walker constellation, such as global coverage with fewer satellites (16 satellites) and lower station keeping fuel consumption.[4]

The ground segment is constructed on both the lunar surface and Earth. The ground segment on Earth is called Master Control Station (MCS) and focuses on satellite monitoring and orbit maintenance operations. The main control station on the lunar surface is called Lunar Control Station (LCS) and is responsible for generating navigation messages. The navigation message includes estimated satellite orbits and clock bias errors that are generated from data sent by Lunar Monitoring Stations (LMS) distributed around the lunar surface. Each LMS is equipped with an LGNSS receiver and atomic clock and collects LGNSS data from navigation satellites. Since LGNSS provides positional information in the lunar fixed frame, user positioning accuracy could be improved by estimating the positioning satellite's orbit using data collected from LMSs fixed in the lunar fixed frame.

Despite the advantages of using the LMSs, to the best of our knowledge, there is no previous research that analyzed the achievable orbit determination error of the navigation satellites by processing the LGNSS signal received at LMSs. In addition, analysis on optimal constellation patterns was limited to case studies on limited orbits, and its optimal configuration has not been comprehensively explored. It is necessary to develop an effective method to simulate the user positioning accuracy for arbitrary satellite and LMS configurations at a low cost to optimize the configuration of the LGNSS.

This paper proposes a method to approximate the user positioning error of LGNSS considering the effects of both satellite constellation and LMS arrangement. In addition, this paper proposes a method to optimize the arrangement of LMSs and satellite constellations. In the proposed optimization method, grid search is performed to search the system comprehensively as possible efficiently. We reduced the search space by using model simplification, assuming symmetrical configurations, and conducting a stepwise optimization to perform the grid search effectively.

2. User Positioning Error

In this section, the error sources of user positioning error in LGNSS are analyzed, and their calculation methods are stated.

2.1. Dilution of Precision

The 3-D root mean square (RMS) position estimation error ΔX_u of a user can be approximated as the product of PDOP (position dilution of precision) and the user range error (URE) σ as follows.

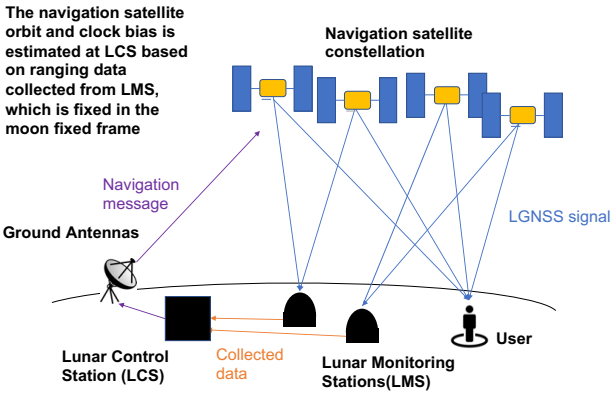

Fig. 1. Overview of the LGNSS system.

$$\Delta X_u = PDOP \times \sigma \tag{1}$$

When n_v satellites are visible, PDOP could be calculated as follows.

$$-\boldsymbol{I}^{(i)} = \frac{1}{||\boldsymbol{x_s^{(i)}} - \boldsymbol{x_u}||}(x_s^{(i)} - x_u, y_s^{(i)} - y_u, z_s^{(i)} - z_u) \tag{2}$$

$$\boldsymbol{G} = \begin{bmatrix} (-\boldsymbol{I}^{(1)})^T & 1 \\ (-\boldsymbol{I}^{(2)})^T & 1 \\ \vdots & \\ (-\boldsymbol{I}^{(n_v)})^T & 1 \end{bmatrix} \tag{3}$$

$$\boldsymbol{H} = (\boldsymbol{G}^T\boldsymbol{G})^{-1} \tag{4}$$

$$PDOP = \sqrt{H_{11} + H_{22} + H_{33}} \tag{5}$$

PDOP is totally dependent on the geometry of satellites with respect to the user, which is described in the geometry matrix, $\boldsymbol{G}$. Eq.(1),(4), and (5) does not provide an accurate error when the UREs among the navigation satellites are not equivalent, but the PDOP value could provide us a good insight about the desirability of satellite geometry for good positioning accuracy. Thus, as mentioned later, PDOP calculations are effective for briefly evaluating the satellite constellation desirability before actual user positioning error evaluation.

2.2. Error Sources of URE

The error sources of the pseudo-range error σ have to be analyzed to approximate the user positioning error. In the case of LGNSS, error sources are much fewer than the terrestrial GNSS because the effect of the tropospheric delay or ionospheric delay does not have to be considered. Therefore, when multi-pass errors are ignored, only three error sources have to be considered:

1. Satellite clock bias
2. Satellite ephemeris (estimated orbital information)
3. Receiver (such as thermal noise, software accuracy)

Since errors produced by 3 depends on the receiver device, we should minimize error sources 1 and 2 (called the signal in space user range error, SIS-URE) when optimizing the LGNSS configuration.

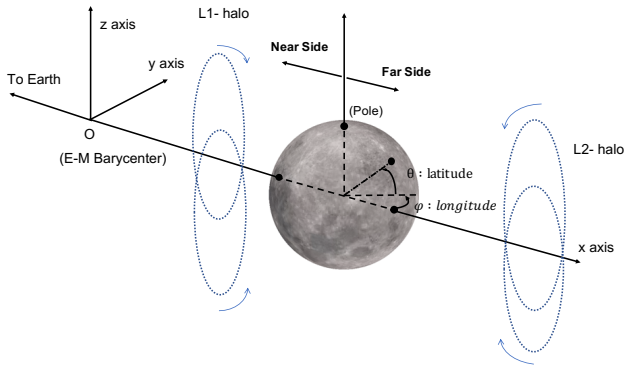

Fig. 2. Earth-Moon fixed rotational frame.

2.3. Orbit and Clock Bias Estimation Errors

Satellite clock and orbit are estimated using the LGNSS signal data collected at the LMSs that are distributed on the lunar surface. Therefore, its arrangement has to be optimized to minimize SIS-URE. In this paper, SIS-URE is approximately evaluated by a covariance study. A Covariance study provides the best possible performance that could be expected.[6)]

2.3.1. Dynamics Model and Coordinate

Before explaining the estimation algorithms, the dynamics model used in this paper is explained. Several assumptions on dynamics as shown below are made to simplify the model to reduce the computational cost.

1. The dynamics of spacecraft motion are approximated by the circular restricted three-body problem (CRTBP). The perturbation from the sun, spherical harmonics, and solar radiation pressure is not considered. However, the process noise is considered in the orbit determination error calculation of navigation satellites.
2. The libration of the Moon is not considered. This assumption means that the surface of the Moon is fixed relative to the Earth-Moon fixed rotational frame.
3. Moon surface topology is not considered. Instead, the elevation mask of 5° is considered when evaluating satellite visibility from observers or LMSs on the lunar surface.

When assumption No.2 is made, the position of the user and LMS on the lunar surface are fixed in the Earth-Moon fixed rotational frame. Therefore, the position and velocity of navigation satellites, users, and LMSs are all defined in the Earth-Moon fixed rotational frame in this paper. The coordinate system and the definition of latitude and longitude on the Moon surface are shown in Fig. 2.

2.3.2. Equation of Motion and Observation Equation

Satellite orbit and clock bias, as well as the LMS position and clock bias, are defined as unknown states and are estimated in the simulation. The state vector for satellite i $\boldsymbol{X}_s^{(i)}$ and state vector for LMS j $\boldsymbol{X}_l^{(j)}$is defined as follows.

$$\boldsymbol{X}_s^{(i)} = \begin{bmatrix} x_s^{(i)} & y_s^{(i)} & z_s^{(i)} & u_s^{(i)} & v_s^{(i)} & w_s^{(i)} & \Delta t_s^{(i)} \end{bmatrix}^T \tag{6}$$

$$\boldsymbol{X}_l^{(j)} = \begin{bmatrix} x_l^{(j)} & y_l^{(j)} & z_l^{(j)} & \Delta t_l^{(j)}. \end{bmatrix}^T \tag{7}$$

When there are N satellites and M LMSs, the state vector is defined as follows

$$\boldsymbol{X} = \begin{bmatrix} \boldsymbol{X}_s^{(1)} & \cdots & \boldsymbol{X}_s^{(N)} & \boldsymbol{X}_l^{(1)} & \cdots & \boldsymbol{X}_l^{(M)} \end{bmatrix}^T. \tag{8}$$

State equation for satellites in CRTBP could be defined as

$$\begin{aligned} &\dot{\boldsymbol{X}}_s^{(i)} \\ &= F(\boldsymbol{X}_s^{(i)}) + \boldsymbol{u} \\ &= \begin{bmatrix} u_s^{(i)} & v_s^{(i)} & w_s^{(i)} & 2v_s^{(i)} - \bar{U}_x & -2u_s^{(i)} - \bar{U}_y & -\bar{U}_z & d\Delta t \end{bmatrix}^T \\ &+ \begin{bmatrix} 0 & 0 & 0 & w & w & w & 0 \end{bmatrix}^T, \end{aligned} \tag{9}$$

$$\dot{\boldsymbol{X}}_l^{(j)} = \begin{bmatrix} 0 & 0 & 0 & d\Delta t \end{bmatrix}^T, \tag{10}$$

where $d\Delta t$ is the changes of clock bias, which is set to 0 in the paper of this simulation. As mentioned before, LMS position is fixed in the rotational frame, when libration is not considered. $\bar{U}$ is the effective potential, and calculated as follows

$$\bar{U} = -\frac{1}{2}(x^2 + y^2) + -\frac{\mu_1}{r_1} - \frac{\mu_2}{r_2} - \frac{1}{2}\mu_1\mu_2, \tag{11}$$

where r_1 and r_2 is the distance between the S/C and the first/second body. The measured pseudo range $\bar{\rho}_k^{(ij)}$ at time ephoch t_k between satellite i and LMS j could be described as

$$\begin{aligned} \bar{\rho}_k^{(ij)} &= \rho_k^{(ij)} + c\Delta t_i \\ &= \sqrt{(x_s^{(i)} - x_l^{(j)})^2 + (y_s^{(i)} - y_l^{(j)})^2 + (z_s^{(i)} - z_l^{(j)})^2} \\ &+ c(\Delta t_s^{(i)} - \Delta t_l^{(j)}) \end{aligned} \tag{12}$$

Thus, when n_{obs} observations are made at time epoch t_k, the observation vector at time epoch t_k, $\dot{\boldsymbol{Y}}_k$ is a $n_{obs} \times 1$ vector that could be written as below

$$\begin{aligned} \dot{\boldsymbol{Y}}_k &= G(\boldsymbol{X}_k) + \boldsymbol{\epsilon}_k \\ &= \begin{bmatrix} \bar{\rho}_k^{(s_i l_j)} \\ \vdots \\ \bar{\rho}_k^{(s_p l_q)} \end{bmatrix} + \boldsymbol{\epsilon}_k \\ &(s_i, \cdots, s_p \in [1, N], \quad s_j, \cdots, l_q \in [1, M]) \end{aligned} \tag{13}$$

State and observation vectors are linearized around the reference state $\boldsymbol{X}^*$ and $\boldsymbol{Y}^*$, as follows

$$\boldsymbol{x} = \boldsymbol{X} - \boldsymbol{X}^*, \ \boldsymbol{y} = \boldsymbol{Y} - \boldsymbol{Y}^* \tag{14}$$

State equation and observation equation are linearized as follows

$$\dot{\boldsymbol{x}}(\boldsymbol{t}) = A(t)\boldsymbol{x}(t) + \boldsymbol{u}(t) \tag{15}$$

$$\boldsymbol{y_i} = \tilde{H}_i \boldsymbol{x_i} + \epsilon_i \tag{16}$$

$$A(t) = \left[\frac{\partial F(t)}{\partial X(t)}\right]^*, \ \tilde{H}_i = \left[\frac{\partial G}{\partial X}\right]^* \tag{17}$$

In this paper, as described in the next chapter, the state is not actually estimated, so these linearizations are done around the true trajectory.

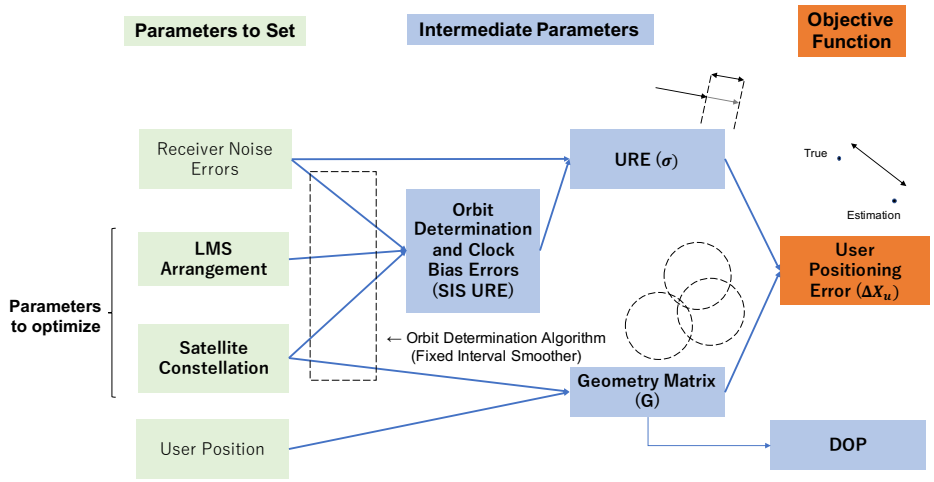

Fig. 3. The relationship between optimization parameters and user positioning error.

2.3.3. Estimation Algorithm: Fixed-Interval Smoother

When estimating the state vector at time t_k, it is desirable to use all observations through time $t_l (l > k)$. To consider the effects of process noise, fixed-interval smoother is applied. In this paper, only the covariance analysis is conducted to evaluate the best estimation performance. The fixed interval smoother consists of 2 processes: forward filtering and backward smoothing sweep.

In the forward filtering process, the time update step and measurement update step are alternately repeated. In the time update step at time t_{k+1}, the covariance matrix $P_{k+1}$is propagated from the previous time step t_k, as follows

$$\begin{aligned}\bar{P}_{k+1} &= E[(\hat{\boldsymbol{x}}_{k+1} - \boldsymbol{x}_{k+1})(\hat{\boldsymbol{x}}_{k+1} - \boldsymbol{x}_{k+1})^T] \\ &= \Phi(t_{k+1}, t_k) P_k \Phi^T(t_{k+1}, t_k) \\ &\quad + \boldsymbol{\Gamma}(t_{K+1}, t_k) Q_k \boldsymbol{\Gamma}^T(t_{K+1}, t_k),\end{aligned} \tag{18}$$

$$\boldsymbol{\Gamma}(t_{K+1}, t_k) = \int_{t_k}^{t_{k+1}} \Phi(t_{k+1}, \tau) B(\tau) d\tau, \tag{19}$$

where Q_k is the process noise covariance matrix and R_k is the observation covariance matrix. After the time update step, measurement updates are conducted, where the covariance matrix is updated using the observed information as follows,

$$P_k = \left(\tilde{H}_k^T R_k^{-1} \tilde{H}_k + \bar{P}_k^{-1}\right)^{-1} \tag{20}$$

In the backward sweep step, the covariance matrix is backproapgated as follows,

$$S_k = P_k^k \Phi^T(t_k, t_{k-1})(P_{k+1}^k)^{-1} \tag{21}$$

$$P_k^l = P_k^k + S_k(P_{k+1}^l - P_{k+1}^k)S_k^T, \tag{22}$$

where P_k^l is the covariance matrix of estimated satellite state, based on observation through t_l. When all of the observation through total simulation time step K is used, $l = K$.

2.4. Calculation of User Positioning Error

As mentioned, when ephemeris error and satellite clock error is not equal for all observed satellite, Eq. (1) could not be directly applied to approximate the user positioning error. Using the Best Linear Unbiased Minimum Variance Estimator (BLUE), the covariance matrix for estimated user state (position and clock bias) could be described as follows.[9)]

$$\boldsymbol{P_u} = (\boldsymbol{G}^T \boldsymbol{R}_{\boldsymbol{URE}}^{-1} \boldsymbol{G})^{-1}, \tag{23}$$

where $\boldsymbol{G}$ is the geometry matrix, and the $\boldsymbol{R_{URE}}$ is the covariance matrix for URE measurements with the observed satellites. When n_{vk} satellites are visible at time step k, geometry matrix G could be calculated as Eq. (4), and$\boldsymbol{R_{URE}}$ could be calculated as follows.

$$\boldsymbol{R_{URE}} = \begin{bmatrix} \sigma_k^{(i)} & 0 & \dots & 0 \\ 0 & \sigma_k^{(i)} & \dots & 0 \\ \vdots & \vdots & \ddots & \vdots \\ 0 & 0 & \dots & \sigma_k^{n_{vk}} \end{bmatrix}, \tag{24}$$

$$\sigma_k^{(i)} = \boldsymbol{P}_{\boldsymbol{R}_k}^{(i)}(1,1) + \bar{\epsilon}_i, \tag{25}$$

$$\boldsymbol{P}_{\boldsymbol{R}_k}^{(i)} = (DCM)\boldsymbol{P}_{\boldsymbol{s}_k}^{(i)}(DCM)^T, \tag{26}$$

where $\boldsymbol{P}_{\boldsymbol{R}_k}^{(i)}$ is the URE between the user and satellite i, and $\bar{\epsilon}_i$ is the error source except satellite OD error, such as satellite/receiver clock bias and receiver noise. This $\bar{\epsilon}_i$ value for all satellites and receiver was set to 1 m. $\boldsymbol{P}_{\boldsymbol{s}_k}^{(i)}$ is the estimated satellite state covariance matrix, that is part of P_k^K in Eq. (22), and DCM is the Direction Cosine Matrix, a rotation matrix that matches the x-axis to the line-of-sight direction vector from the user to the satellite.

From the covariance matrix $\boldsymbol{P_u}$ in Eq. (23), 3-D RMS positioning error Δx_u considering the SIS-URE for each navigation satellite could be calculated as follows.

$$\Delta X_u = \sqrt{P_{u(11)} + P_{u(22)} + P_{u(33)}} \tag{27}$$

This is the target parameter that should be minimized. The relationship of the satellite constellation, LMS arrangement and the user positioning error is shown in Fig.3.

3. Optimization Method

3.1. Design Parameter of LGNSS

In this section, design parameters to define the constellation and LMS arrangement are stated. To provide equal positioning service over the globe, a symmetrical configuration for navigation satellite constellation and LMS arrangement is assumed.

Table 1. Design parameters for the proposed constellation.

symbol	parameter description
r_{ph}	the perilune radius of halo orbits
r_{pd}	the perilune radius of DRO
n_h	the number of satellites in each halo orbit
n_d	the number of satellites in DRO
$\Delta\psi_{L12}$	the difference of phase angles of satellites in L1 and L2 north halo orbits
$\Delta\psi_{NS}$	the difference of phase angles of satellites in north and south halo orbits for both L1 and L2

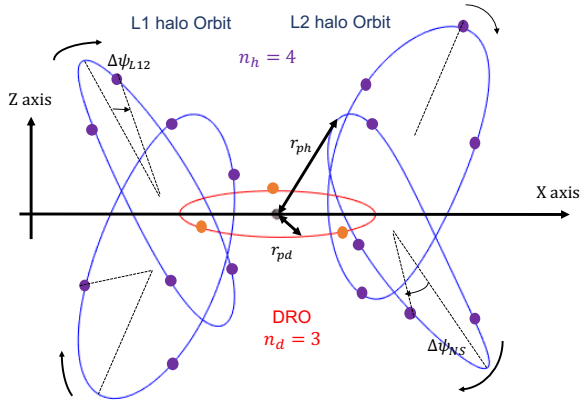

Fig. 4. Overview and design parameters of the proposed constellation. The figure shows the case of $n_h = 4$ and $n_d = 3$.

3.1.1. Orbits for Constellation

In this research, a constellation that exploits north and south halo orbits around L1 and L2 Lagrange points is used as a basic design for the constellation. Benefits of using this constellation are mentioned in the work of Circi and Romagnoli, such as global coverage with as few as 16 satellites in total, low orbital station-keeping fuel consumption, and the continuous communication path to the Earth. In this paper, in addition to this basic constellation, the use of distant retrograde orbit (DROs) is also proposed as an option. DRO is a stable periodic orbit in the planar circular restricted three-body problem (PCRTBP) and is a retrograde orbit around the Moon in the rotating frame. The DRO orbiting on the equatorial plane is expected to mitigate the limited coverage of low-latitude regions from halo orbits.

Halo orbit and DRO families for this research are generated using the pseudo-arclength continuation method.[2] Generated periodic orbits (Northern halo orbits and DROs) are shown in Figs. 5,6, and 7 with the orbital period and the z amplitude (A_z).

3.1.2. Design Parameters of Constellation

In this paper, as the concept of Walker's Constellation, we aim to provide similar positioning services across the globe. Thus, we consider a symmetrical constellation that covers the whole globe as equally as possible. Therefore, an equal number of satellites are deployed in each halo orbit, and the perilune radius of all halo orbits is set equal. The phase angles of satellites in the same orbital plane are separated equally to maximize the spatial separation of the satellites in each orbit plane. Based on these assumptions, the constellation could be defined by the design parameters listed in Table 1. The overview and the design parameters of the proposed constellation are shown in Fig. 4.

If the phase separation between north and south halo orbits ($\Delta\psi_{NS}$) is set around 0, the satellites at north and south halo orbit come close at the intersection point of the north and south halo orbit. This causes the overlap of two satellites from the user's point of view and leads to a degrading in DOP values. Changing $\Delta\psi_{NS}$ has an effect on low to middle latitude regions, where navigation satellites on both north and south halo orbits are visible. On the contrary, phase separation between L1 and L2 halo orbits ($\Delta\psi_{L12}$) affects positioning performance on high latitude regions, where navigation satellites on both L1 and L2 halo orbits are visible. Although these phase separation parameters affect user positioning performances, the optimization of these phase separation parameters is outside the scope of this paper to prevent the problem from becoming too complicated. Both $\Delta\psi_{NS}$ and $\Delta\psi_{L12}$ are fixed to 0 in this paper. Thus, in this paper, r_{ph}, r_{pd}, n_h, n_d are the optimization variables for constellation optimization.

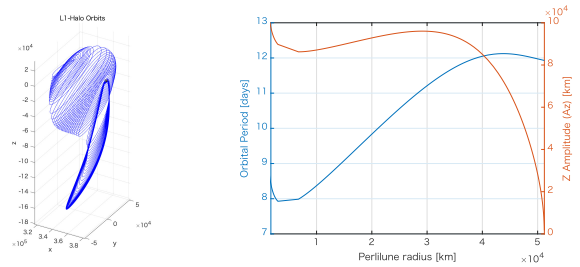

Fig. 5. L1 halo orbit families.

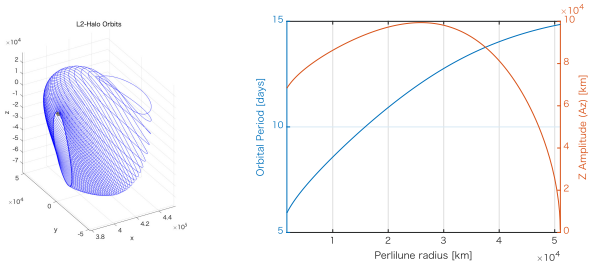

Fig. 6. L2 halo orbit families.

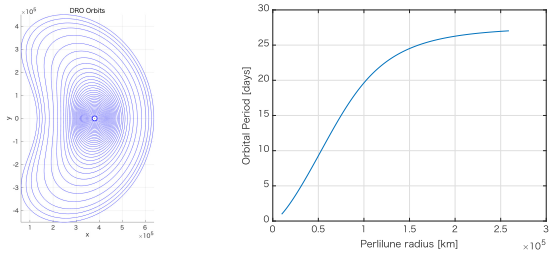

Fig. 7. Distant Retrograde Orbit (DRO) families.

3.1.3. LMS Arrangement

Since the Moon has no ocean, the degree of freedom of the place where the base station can be located in the LGNSS is higher than the monitoring stations for the GNSS of Earth. In this paper, corresponding to the symmetrical arrangement of the navigation satellites, we arranged 8 LMSs symmetrically on the lunar surface, to form an X-shape that intersects in the center of the front side and the far side of the Moon, as shown in Fig. 8. By this assumption, the parameters defining the LMS arrangement are reduced to 2 parameters, which is the absolute of the latitude of LMS: θ_l, and the absolute of the longitude of the LMS at the far side of the Moon: ϕ_l.

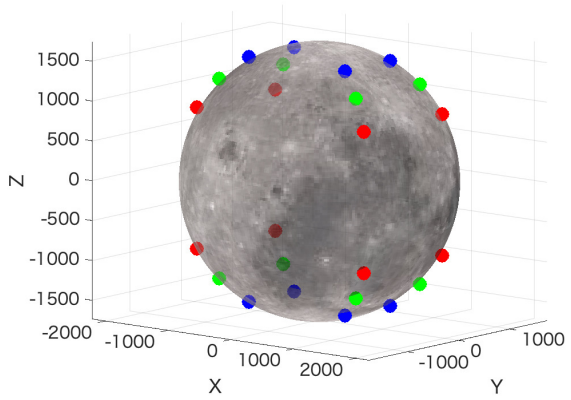

Fig. 8. Three examples of the arrangement of the LMS. Each color shows one arrangement example. In this paper, the LMSs are arranged to form an X-shape at both surfaces of the Moon.

3.2. Optimization Problem Definition

Given the above assumptions, the optimization problem of the satellite and LMS arrangement to minimize user error with the given navigation satellite and LMS number could be formulated as follows.

$$\begin{aligned} \min : J &= \frac{1}{K} \cdot \frac{1}{U} \sum_{k=1}^{K} \left(\sum_{u=1}^{U} \Delta X_u(n_h, n_d, \theta_l, \phi_l, u, k) \right) \\ \text{find} : & \; n_h, n_d, r_{ph}, \phi_l, \theta_l \\ \text{s.t} : & \; 4n_h + n_d = N, \\ & \; r_{ph_{min}} \leq r_{ph}, \leq r_{ph_{max}}, \\ & \; M = 8, \\ & \; 0 \leq \phi_l \leq \pi/2, 0 \leq \theta_l \leq \pi/2, \end{aligned} \tag{28}$$

where K is the number of time steps, and U is the number of user point s to evaluate the positioning error. $r_{ph_{min}}$ indicates the minimum perilune radius permitted, which is identical to the radius of the Moon (=1737 km), and $r_{ph_{max}}$ is the maximum perilune radius which is set considering the region in which each periodic orbits could exist ($r_{ph_{max}} = 5 \times 10^4$ km for halo orbits).

Occasionally, the satellite may overlap from the viewpoint of the user. This causes the fall of the rank of the geometric matrix, and the user positioning error may diverge. In these cases, the ΔX_u value for that user position at that time step is ignored and is not included in the objective function calculation. Since this is a temporary phenomenon, even in consideration of actual use, it is possible to deal with this problem by waiting for a while until the satellite moves or using an estimated value on the user side.

3.3. Optimization Procedure

Although the optimization problem is somewhat simplified by reducing parameters by assuming symmetrical configurations, the optimization problem expressed by Equation (28) is a complicated problem for the following reasons.

- As shown in Fig.3, the satellite constellation affects the objective function (mean user positioning error) through 2 different intermediate parameters, URE, and the geometry matrix.
- It is a nonlinear optimization problem with mixed-integer and continuous optimization variables.
- The changes of visibility of satellites from a user point or LMS are stepwise, making it difficult to calculate the gradients of the variables.

One possible solution to this type of problem is to use metaheuristics, such as a genetic algorithm or particle swarm optimization. These algorithms could provide relatively good solutions with small computational efforts. However, metaheuristics do not guarantee that the solution converges to the optimal solution, except for some limited problems.[5] Besides, when considering this optimization as part of a conceptual design, the important purpose of optimization is to obtain an understanding of the features of the problem through optimization rather than finding the exact optimal solution itself. Therefore, in this paper, a grid search is conducted to explore a wide portion of the solution space comprehensively. A sub-optimal solution is obtained by gradually narrowing down the candidates of the solution by carrying out a stepwise grid search from the parameters that are sensitive to the user positioning error.

Grid search has to be performed within 5 parameters: $n_h, r_{ph}, r_{pd}, \theta_l$ and ϕ_l. However, by simulation, it was found that the DRO perilune radius had almost no sensitivity on the PDOP value, and thus r_{pd} is fixed to 3.0×10^4 km in this paper. Therefore, the grid search was conducted with the remaining four parameters in the following steps.

Step1: Satellite Distribution:
: For each given number of satellites, distribute the satellites to each orbit so as to satisfy the condition. Perform the following operations for each of the obtained combinations, (n_h, n_d).

Step2: Selection by Visibility:
: Perform a grid search within r_{ph}. For each (n_h, n_d, r_{ph}) , compute the percentage of time when the visible satellite number is 4 or more (t_v). Judge if t_v exceeds the threshold value ($\bar{t}_v$) set by the user, and constellations that exceeds the threshold go on to the next step.

Step3: Selection by PDOP:
: For each of the possible constellation obtained in Step2, calculate the PDOP average over simulation time, and find a r_{ph} value that minimizes the PDOP value for each (n_h, n_d) pairs. The obtained (n_h, n_d, r_{ph}) pair goes to the next step.

Step4: LMS Arrangement Optimization:
: For each of (n_h, n_d, r_{ph}) obtained in Step2, perform a grid search within ϕ_l and θ_l. Find the $(n_h, n_d, r_{ph}, \phi_l, \theta_l)$ pairs that minimizes the average user measurement error.

The arrangement of the LMSs for each orbit was optimized after narrowing down the candidates for the trajectory because the sensitivity of the perilune radius (or orbit) with respect to the user positioning error is found to be higher than the sensitivity of LMS arrangement via orbit determination error. The objective of this method is to reduce the computational cost by narrowing down the solution using intermediate parameters that are easy to calculate, such as satellite visibility and PDOP. The actual user positioning error, which is computationally heavy, is actually computed only at the final LMS optimization step to evaluate the preference of LMS arrangement, which could not be evaluated by intermediate parameters.

The disadvantage of this method is that it is not considering the effect on r_p to user positioning errors via orbit determination

errors. This disadvantage could be lessened by passing several r_{ph} values to Step 4, but this is not conducted in this paper.

4. Result

The proposed method was tested for the case of 20 satellites with 8 LMSs.

4.1. Simulation Conditions

The assumed condition for optimization is listed in Table. 2.

Table 2. Simulation conditions

Parameter	Value
elevation musk	5°
simulation time	60 days
simulation time interval	10 min
process noise on acceleration (1σ)	1×10^{-9} m/s^2
range error (1σ)	1 m
[initial state estimation errors]	
error in satellite position error (1σ)	1000 m
error in satellite velocity error (1σ)	1 m/s
error in satellite clock bias (1σ)	1.0×10^{-9} s
error in LMS clock bias (1σ)	1.0×10^{-9} s
error in LMS position (1σ)	1 m

The user positioning performance is evaluated at discrete time steps and user position. Simulation time should be as long as the geometrical repetitive period of the constellation. For each periodic orbit i, the repetitive period ${T_{rep}}^{(i)}$ could be calculated as follows.

$$T_{rep}^{(i)} = T_p^{(i)}/n_i, \tag{29}$$

where $T_p^{(i)}$ indicates the revolution of the orbit. From Fig. 5, 6 and 7, T_{rep} would not exceed 10 days if more than 3 satellites are added to each orbit. Since the orbital period of each orbit is different in L1-halo, L2-halo, and DRO mixed constellation, it is hard to define the geometrical repetitive period. Thus, the simulation time is set as 60 days.

We arranged 42 evaluation points at the vertex of the geodesic dome to evaluate the user positioning error on the surface. The location of the evaluation points is shown in Fig. 9.

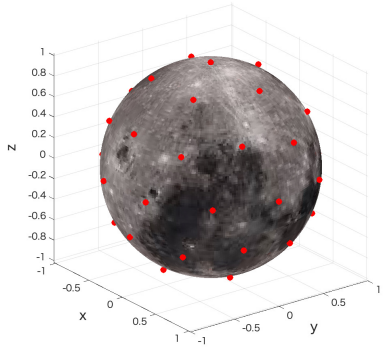

Fig. 9. Position of the user (-x : to Earth)

4.2. Satellite Distribution

For the constellation with 20 satellites, there are five types of possible constellation patters as shown below:

C1: $n_h = 5$ $n_d = 0$
C2: $n_h = 4$ $n_d = 4$
C3: $n_h = 3$ $n_d = 8$
C4: $n_h = 2$ $n_d = 12$
C5: $n_h = 1$ $n_d = 16$

For C5, it is obvious that the coverage of the pole regions could not be achieved because pole regions could not be seen from navigation satellites on DRO. Therefore, constellation types C1 - C4 are set as candidates.

4.3. Visibility Analysis

Fig. 10 shows the ratio of time that more than four satellites are seen from the lunar surface. Only C1 and C2 had 100% visibility in every perilune radius. C3 also had good visibility when perilune radius is in between 1×10^4 km to 3×10^4 km, but continuous visibility of four or more navigation satellites is not achieved when the perilune radius exceeds 3.2×10^4 km, as shown in Fig. 10b. This is because the z amplitude of both L1 and L2 halo orbit drops rapidly as shown in Figs. 5 and 6. Furthermore, when the number of satellites in each halo orbit is below 3, such as the C4 constellation, whatever the perilune radius of the halo orbit, the number of satellites in the halo orbit is not sufficient to provide continuous visibility of 4 navigation satellites on the pole. The pole region is an important target in lunar exploration because the presence of water is anticipated. Therefore, constellations that could not cover the polar regions may not be preferable in actual use.

4.4. PDOP Analysis

PDOP is calculated for constellations that the t_v value exceeded 0.99. Table. 3 and Fig. 11 shows the result of the PDOP analysis. For C1 (Fig. 11a), the transition of the PDOP in the low latitude area on the front and back surface becomes sharp V shape, while the PDOP of the pole is remained low in wide range of perilune radius. On the contrary, for C3(Fig. 11c), the transition of the PDOP in the pole is V-shaped, while PDOP is remained low in a wide range of halo orbit perilune radius. PDOP of C2 type constellation is remained low in various latitude regions for a wide range of halo orbit perilune radius. For the global average of PDOP, C2 had the best value among the four constellations shown in Table. 3.

Global distribution of the PDOP at the far side of the Moon for C1, C2, and C3 type constellation when perilune radius is set to minimize the global average is shown in Fig. 12. While the constellation with only halo orbits has good PDOP values on pole regions, they do not have good PDOPs on low altitude regions. This is due to the large z amplitude of halo orbits. In the sky of the user at low altitude regions, all navigation satellites on halo orbit appear near the horizon, which leads to high DOP values. This problem could be solved by adding satellites to the DRO and providing satellites in high elevation directions in the user's sky.

From Fig. 11, it could be said that there are additional advantages in halo - DRO mixed constellations. In C2 and C3, PDOP values remain low (under 2) in regions where halo orbit perilune radius is shorter than 2.0×10^4 km. This is because the satellites in DRO could compensate for the degradation in

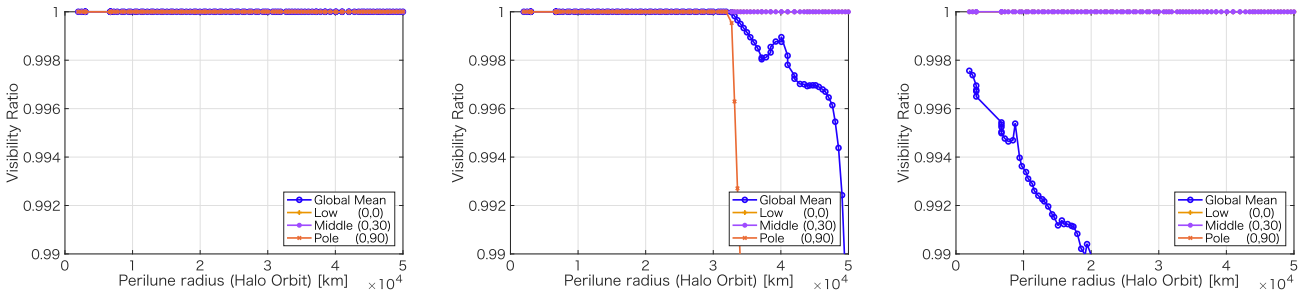

(a) C1,C2 : $(n_h, n_d) = (5, 0), (4, 4)$ (b) C3: $(n_h, n_d) = (3, 8)$ (c) C4: $(n_h, n_d) = (2, 12)$

Fig. 10. The ratio of time that 4 or more satellites are seen. The label 'global' shows the global average, while 'Low', 'Middle', and 'Pole' label shows the value at the user point (longitude, latitude) = (0,π/2),(0,0),(π,0). The visibility of the pole degrades as the halo orbit perilune radius gets long, when $n_h \leqq 3$.

Table 3. Minimum global PDOP value and for constellation type C1-C4. 'perilune radius' shows the halo orbit perilune radius that minimizes the PDOP global average. Best and worst local PDOP values with the user position are shown as well.

Constellation (n_h, n_d)	Perilune Radius [km]	global mean	best local PDOP (lon, lat)	worst local PDOP (lon,lat)
C1 (5,0)	2.20×10^4 km	2.01	1.66 (W126,N27)	3.56 (E180,N0)
C2 (4,4)	2.05×10^4 km	1.85	1.62 (E18,N58)	2.44 (E0,N90)
C3 (3,8)	2.38×10^4 km	1.88	1.59 (E0,N0)	3.88 (E0,N90)
C4 (2,12)	1.94×10^4 km	2.54	1.55 (E0,N0)	15.72 (E0,S90)

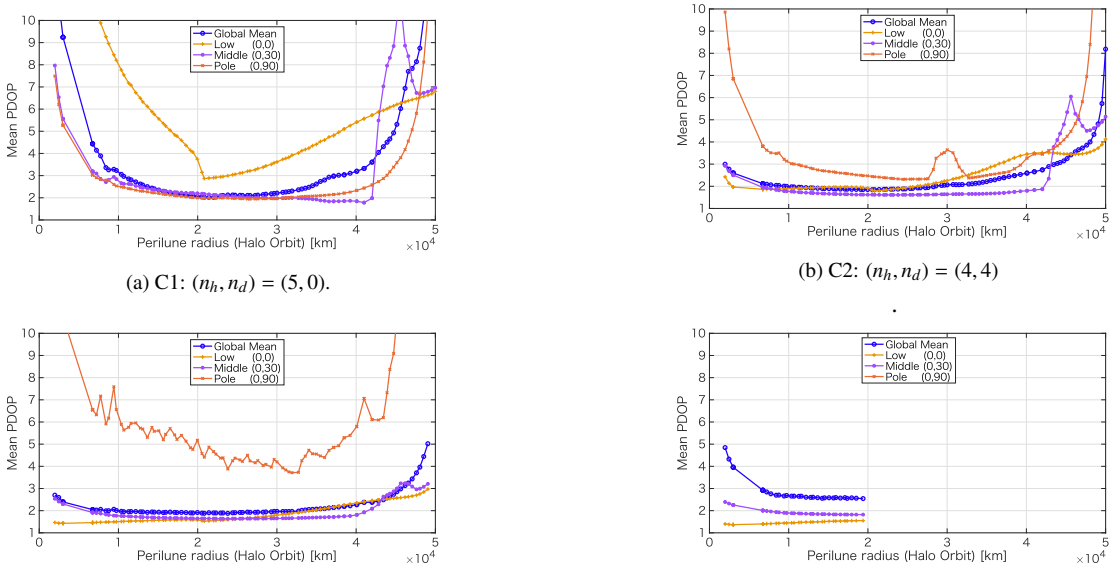

(a) C1: $(n_h, n_d) = (5, 0)$. (b) C2: $(n_h, n_d) = (4, 4)$

(c) C3: $(n_h, n_d) = (3, 8)$. (d) C4: $(n_h, n_d) = (2, 12)$.

Fig. 11. Global average of PDOP when halo orbit radius are changed.

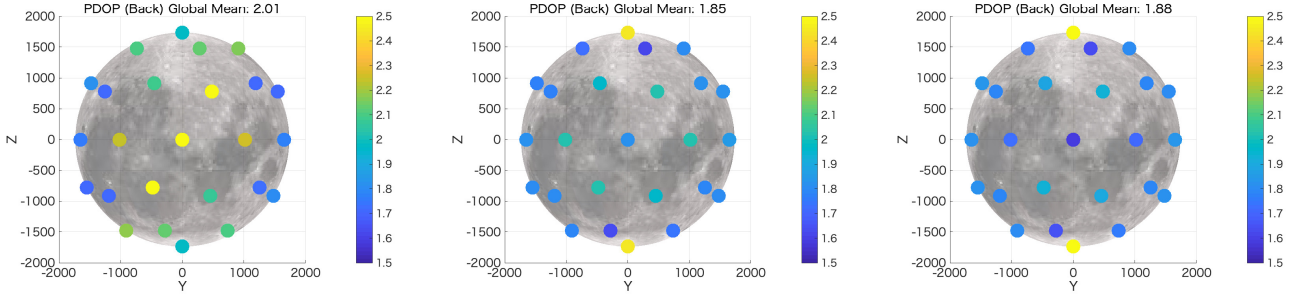

(a) C1: $(n_h, n_d) = (5, 0)$. (b) C2: $(n_h, n_d) = (4, 4)$. (c) C3: $(n_h, n_d) = (3, 8)$.

Fig. 12. Global distribution of PDOP (mean value) on the far side of the lunar surface when r_{ph} is chosen to minimize the global mean PDOP value. PDOP in the pole is lowered as more satellites are distributed to halo orbits, but the PDOP value tends to be high in low latitude region without DRO.

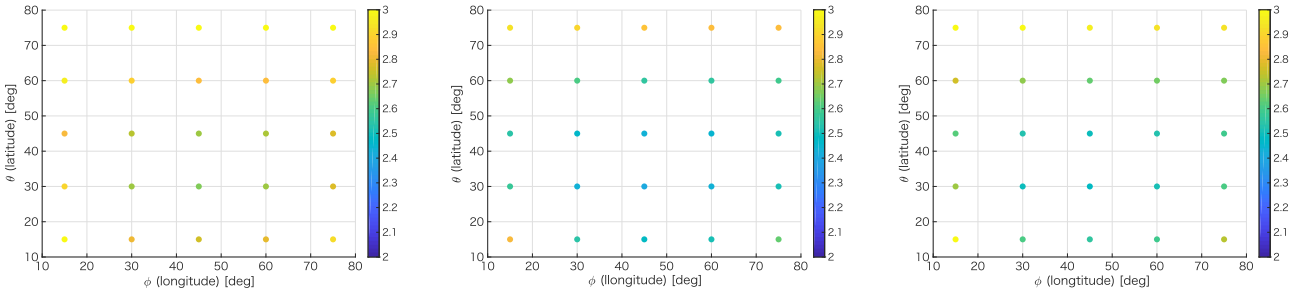

(a) C1: $(n_h, n_d) = (5, 0)$. (b) C2: $(n_h, n_d) = (4, 4)$. (c) C3: $(n_h, n_d) = (3, 8)$.

Fig. 13. User measurement errors [m] when LMS arrangement parameter (θ_l,ϕ_l) are changed.

Table 4. The obtainded optimal configuration for each constallation types. The global mean of the user positioning error (1 σ) is shown as well. The global mean of user positioning error was minimized when 4 satellites are distributed at each orbit, and LMS is placed in $(\theta_l,\phi_l) = (\pi/4, \pi/6)$.

Constellation	Perilune radius [km]	LMS position (θ_l(lat),ϕ_l(lon))	User positioning error [m] (1 σ)
C1 (5,0)	2.20×10^4 km	$\theta_l = 45[deg],\ \phi_l = 30[deg]$	2.67
C2 (4,4)	2.05×10^4 km	$\theta_l = 45[deg],\ \phi_l = 30[deg]$	2.40
C3 (3,8)	2.38×10^4 km	$\theta_l = 45[deg],\ \phi_l = 30[deg]$	2.47

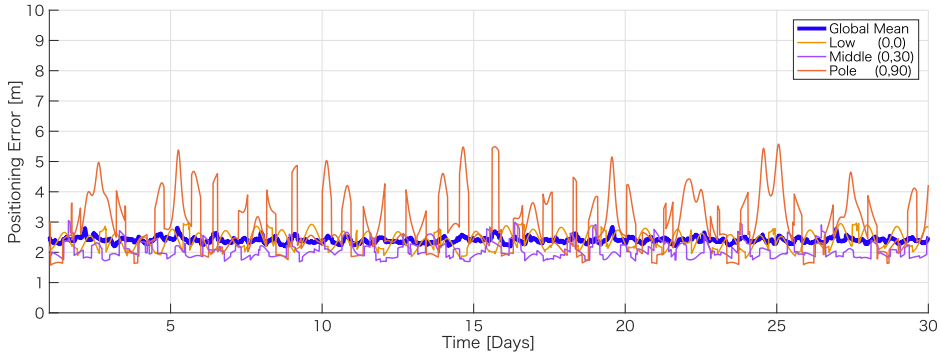

Fig. 14. User positioning error transition for 30 days of C2 optimized configuration.

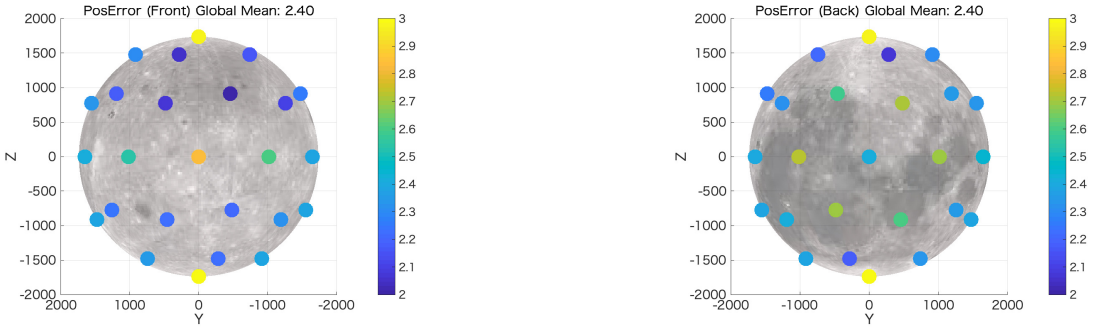

(a) Front Surface. (b) Back Surface.

Fig. 15. Positioning error [m] distribution for optimized configuration of C2.

PDOP at low altitude areas when halo orbits that have large z amplitude are used. These halo orbits are called Near Rectilinear Halo Orbits (NRHOs) and are a stable orbit in a linear sense in the CRTBP.[1)] Few propellant resources are required to (theoretically) maintain the NRHOs and thus, we can extend the service providing period by using these orbits. DRO is also a linearly stable orbit, so the combination of NRHO and DRO could be a preferable candidate for the LGNSS navigation satellite constellation.

4.5. LMS Arrangement

The constellation that had the lowest PDOP value in constellation type C1, C2, and C3 were chosen as a target constellation for LMS arrangement optimization. Figure. 13 shows the result of LMS arrangement optimization. The grid search results showed that for all three types of constellations, user positioning errors are minimized when LMS is placed at mid-latitude and mid-longitude regions, where LMSs are spatially separated on the lunar surface.

The optimized configuration for C1, C2, and C3 is shown in

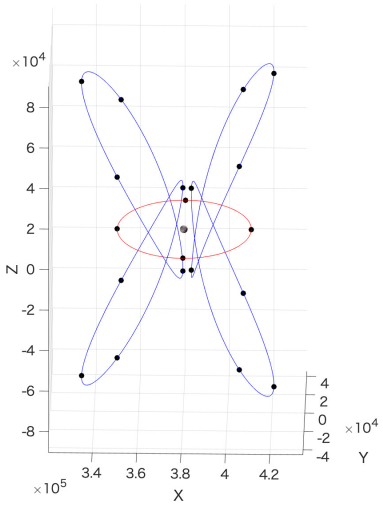

Fig. 16. The overview of the optimized constellation.

Table. 4. The minimum user positioning error is achieved in the C2 constellation with $r_h = 2.05 \times 10^4$ km.

4.6. Performance of optimized configuration

This section describes the performance of the optimized configuration in detail. The overview of the constellation is shown in Fig. 16. Figure. 14 shows the transition of the global user positioning accuracy within half of the simulation time (30 days), and Fig. 15 shows the distribution of the average user positioning error on the front side and the far side of the Moon. For optimized constellation, user positioning errors below 3m for 1 σ, and below 10m for 3 σ are achieved at mid-latitude regions. On the contrary, user positioning performance at the pole is not good compared with other regions. This could be improved by adding more navigation satellites on halo orbits.

The optimization result indicates that in LGNSS, sub-decimeter user positioning may be achieved with fewer satellites compared with terrestrial GNSS since there is no tropospheric delay nor ionospheric delay. However, as mentioned before, it should be noted that the evaluated user positioning error is a result of covariance analysis and shows the best possible performance. Monte-Carlo simulations in the Ephemeris model has to be conducted to simulate the user measurement error more accurately.

5. Conclusion

In this paper, the error source for LGNSS was analyzed, and the method to evaluate the user positioning performance considering both navigation satellite and LMS was proposed. Using the proposed user positioning error evaluation method, we formulated the satellite constellation and LMS arrangement optimization problem that minimizes the mean user positioning error. In the proposed optimization method, a sub-optimal solution is obtained by gradually narrowing down the candidates of the solution with stepwise grid search in the following order: visibility analysis, PDOP analysis, and user positioning error analysis. The proposed method is applied to the optimization problem of the constellation of 20 satellites and an arrangement of 8 LMSs. The result showed that by deploying the satellite in both DRO and halo orbit, the PDOP in the low latitude region is reduced, and thus lower user positioning error is achieved compared with the constellation with satellites only on halo orbits. The result of the PDOP analysis also suggested that the navigation satellite constellation could be formed by using only highly stable orbits, NRHOs and DRO. The X-shaped LMS arrangement is assumed in this paper, and results showed that placing the LMS in intermediate latitude and longitude is preferable for minimizing user positioning error. In the optimal configuration, the global mean user positioning accuracy of 10 m (3σ) or less was achieved.

Future works will focus on optimizing other constellation parameters, including phase separation angles and other LMS arrangement patterns. We are also planning to assess the navigation performance in the N-body Ephemeris model. The proposed optimization method and the obtained result of this paper could be used to effectively select and evaluate the candidate configurations for the preliminary design of LGNSS.

Acknowledgments

I am grateful for Prof. Nakasuka and Associate Prof. Funase for their support and advice for this study. I would also like to thank Assistant Prof. Ikari for giving me insightful and constructive comments regarding the model construction for the LGNSS simulator. Finally, I am grateful to Dr. Kawabata for offering me useful advice regarding orbit determination model construction. Without their guidance and advice, this paper would not have been possible.

References

1) Zimovan, E. M.: Characteristics and Design Strategies for Near Rectilinear Halo Orbits within the Earth-Moon System, Master Thesis, Purdue University, 2017.
2) Doedel, E.J., paffenroth, R.C., Keller, H.B., Dichmann, D.J., Galàn-Vioque, and Vanderbauwhede, A. : Computation of Periodic Solutions of Conservative Systems with Application to the 3-Body Problem, International Journal of Bifurcation and Chaos **13** (2003), pp. 1353–1381
3) Wijnen, M., Agüera-Lopez, N., Correyero-Plaza, Sara. and Perez-Grande, Daniel.: CubeSat Lunar Positioning System Enabled by Novel On-Board Electric Propulsion, *Plasma Science, IEEE Transacions on.*, **46** (2018), pp. 319–329
4) Circi, C. and Romagnoli, D.: Halo Orbit Dynamics and Properties for a lunar global positioning system design, *MNRAS.*, **442** (2014), pp. 3511–3527.
5) Blum, C., and Roli, A.,:Metaheuristics in combinatorial optimization: Overview and Conceptual Comparison **35** (2003), pp. 268–308
6) Chen,H., Liu, L., Meng, Y., Xu, Z., Long L., Liu, J. : Preliminary Mission Design and Analysis of a Lunar Far-side Positioning CubeSat Mission, 31st International Symposium on Space Technology and Science, Matsuyama, Japan, 2017-d-160p, 2017.
7) Tapley, B. D., Schutz, B. E., and Born, G. H. : *Statistical Orbit Determination*, Elsevier Academic Press, Burlington, MA, 2004.
8) Carretero, S.G.: Study of a lunar satellite navigation system, Master Thesis, Universitat Politécnica de catalunya, 2012.
9) Fletcher, K. *GNSS Data Processing, Vol. I: Fundamentals and Algorithms*, ESA Communications, Noordwijk, 2013, pp. 143–144.